
Anomaly detection in time-series via inductive biases in the latent space of conditional normalizing flows

David Baumgartner

Department of Computer Science
Norwegian University of Science and Technology
Trondheim, Norway
david.baumgartner@ntnu.no

Eliezer de Souza da Silva

BCAM – Basque Center for Applied Mathematics
University of Coimbra, CISUC/LASI, DEI
Coimbra, Portugal
eliezer.silva@uc.pt

Iñigo Urteaga

BCAM — Basque Center for Applied Mathematics
IKERBASQUE — Basque Foundation for Science
Bilbao, Spain
iurteaga@bcamath.org

Abstract

Deep generative models for anomaly detection in multivariate time-series are typically trained by maximizing data likelihood. However, likelihood in observation space measures marginal density rather than conformity to structured temporal dynamics, and therefore can assign high probability to anomalous or out-of-distribution samples. We address this structural limitation by relocating the notion of anomaly to a prescribed latent space. We introduce explicit inductive biases in conditional normalizing flows, modeling time-series observations within a discrete-time state-space framework that constrains latent representations to evolve according to prescribed temporal dynamics. Under this formulation, expected behavior corresponds to compliance with a specified distribution over latent trajectories, while anomalies are defined as violations of these dynamics. Anomaly detection is consequently reduced to a statistically grounded compliance test, such that observations are mapped to latent space and evaluated via goodness-of-fit tests against the prescribed latent evolution. This yields a principled decision rule that remains effective even in regions of high observation likelihood. Experiments on synthetic and real-world time-series demonstrate reliable detection of anomalies in frequency, amplitude, and observation noise, while providing interpretable diagnostics of model compliance.

1 Introduction

Anomaly detection (AD), also known as outlier or novelty detection, is a fundamental problem in signal processing and machine learning with applications ranging from fraud detection and predictive maintenance to medical imaging and network security [Chandola et al., 2009, Pimentel et al., 2014]. Anomaly detection for time-series have temporal dependence that introduces additional com-

plexity, requiring methods that distinguish structured deviations from expected dynamics [Schmidl et al., 2022].

Classical AD typically relies on hand crafted anomaly scores, such as reconstruction error, distance to cluster centers, or density estimates, which must be converted into binary decisions via manually chosen thresholds. In practice, these thresholds are often tuned using labeled examples of anomalous behavior or extensive domain expertise, which can be costly, brittle across domains, and difficult to justify statistically when anomalies are inherently rare and heterogeneous [Chandola et al., 2009].

In many realistic settings, annotated anomalies are scarce or unavailable, whereas large amounts of data describing *expected behavior* can be collected at low cost. This motivates unsupervised anomaly detection, where the learning algorithm is trained on data representing expected behavior and must infer deviations without explicit supervision [Pimentel et al., 2014]. In this setup, the objective is to learn an inherent notion of what constitutes expected behavior directly from data, so that deviations from this learned notion can be flagged as anomalies.

Formally, we posit a parametric generative model with density $p_\theta(\mathbf{x})$ encoding the *expected behavior* into a region of the data space with a well defined statistical distribution $p_\theta(\cdot)$, with samples outside of that region regarded as out-of-distribution (OOD) or anomalous. With this probabilistic framework, anomalies can be scored via quantities intrinsic to the generative model, such as likelihoods, reconstruction-based discrepancies, or hybrid criteria that combine data and latent-space representations. Crucially, this also allows us to develop an approach for AD using goodness-of-fit (GOF) statistical tests.

Modern deep generative models (DPMs) provide flexible parametric families for approximating complex data distributions and have become popular building blocks for probabilistic modeling [Goodfellow et al., 2014, Kingma and Welling, 2022]. Recent studies demonstrate the effectiveness of and interest in unsupervised DPMs for AD across domains [Pang et al., 2021, Xia et al., 2022, Berahmand et al., 2024]. However, these models are not free of pitfalls: recent work on OOD detection has revealed that deep generative models can behave counterintuitively [Serrà et al., 2019, Li et al., 2025], sometimes assigning higher likelihoods to OOD inputs than to in-distribution data. Notably, Morningstar et al. [2021] cautioned us against the naive use of negative log-likelihood (NLL) as a proxy for *typicality*, highlighting the importance of appropriate inductive biases and model diagnostics for AD [Zhang et al., 2021]. These shortcomings reveal a need for generative models that not only fit the nominal data distribution well, but also induce a robust and interpretable separation between expected and unexpected patterns. As argued by Li et al. [2025], likelihood-based training alone does not provide an inherent notion of unexpected behavior, and that such distinctions must arise from explicit structural inductive biases encoded in the model.

In this work, we propose an unsupervised, state-space probabilistic framework for time-series data and study how inductive biases in representation-space can overcome some of these limitations. Specifically, we define a normalizing-flow-based DPM with explicit inductive biases to capture the expected behavior of data via latent, prescribed dynamics. Conditioned on a successful training procedure, the framework provides an inherent (statistical) definition of expected (in-distribution) versus anomalous (out-of-distribution) behavior, enabling unsupervised anomaly detection.

Our contributions include:

- A state-space deep generative model that couples a conditional normalizing flow with explicit (e.g., linear-Gaussian) latent dynamics, constraining observations to map to a temporally coherent, latent trajectories of prescribed density.
- A statistically principled, unsupervised (i.e., label- and threshold-free) anomaly detector based on a goodness-of-fit (e.g., a multivariate Kolmogorov-Smirnov) test in latent space, capable of identifying anomalies even in high-density regions of the DPM.
- A built-in, compliance diagnostic to identify when the DPM training procedure is successful in enforcing the prescribed inductive bias, explicitly signaling when the unsupervised AD procedure is ready for testing.
- Showcasing empirically (i) the in-distribution AD issues with negative log-likelihood-based scores, (ii) the robustness and detection accuracy of the proposed framework, and (iii) its successful performance in-par with established baselines on real-data AD scenarios.

2 Background and Related Work

We provide the necessary background on AD and normalizing flows, situating our work within the existing literature.

Anomaly, outlier, and OOD detection all aim to identify patterns in data that deviate from expected behavior [Ruff et al., 2021, Chandola et al., 2009]. Deep generative models have been widely explored across this and other domains over the last few years [Pang et al., 2021, Xia et al., 2022, Behrmand et al., 2024]. Specifically, time-series anomaly detection (TSAD) deals with connected and ordered data points over time, which yields additional AD challenges. Schmidl et al. [2022] provide a good overview of the complexities inherent in TSAD and the existing approaches to addressing it. Sørnbø and Ruocco [2024] further highlight metrics used in this domain and point out issues that make fair comparisons across methods difficult. VAE based DPM methods for AD often use reconstruction probability or related likelihood surrogates as anomaly scores, enabling a more principled interpretation than ad hoc error thresholds [Xu et al., 2018]. Similarly, GAN-based approaches such as TadGAN [Geiger et al., 2020] or USAD [Audibert et al., 2020] employ sequence-to-sequence generators and critics to reconstruct time-series, deriving anomaly scores from reconstruction residuals and critic responses, highlighting anomalous segments rather than isolated point outliers.

Normalizing flows (NF) are generative probabilistic models that learn a bijective transformation that maps the data to a known distribution [Papamakarios et al., 2021]. These models enable both model fitting and sample generation; i.e., NFs can efficiently compute the log-likelihood of observations ($\log p(\mathbf{x})$) and generate new data ($\mathbf{x} \sim F^{-1}(\mathcal{N}(\cdot))$), which requires tractable Jacobian determinants. We denote the normalizing and likelihood of a data point \mathbf{x} as $p(\mathbf{z} = F(\mathbf{x}))$ and the generation of a data point $\mathbf{x} = F^{-1}(\mathbf{z} \sim \mathcal{N}(\cdot))$, where $F(\cdot; \theta)$ is the NF with parameters θ which we omit when it is clear from the context.

To model multivariate time-series data, we employ conditional normalizing flows (CNF) [Rasul et al., 2020]. NFs can be conditioned in different ways; in this case, we focus on transformation-layer conditioning. This setting requires paired inputs for the CNF, i.e., $F(\mathbf{x} | \mathbf{d}) : \mathbb{R}^D \times \mathbb{R}^M \rightarrow \mathbb{R}^D$. Notice that $\mathbf{d} \in \mathbb{R}^M$ can have different dimension than \mathbf{x} . Unsupervised training of CNF is performed using the data’s negative log-likelihood, according to a base distribution and the change-of-variable formula, with loss function $\mathcal{L}(\mathbf{x}, \mathbf{d}) = \log p(F(\mathbf{x} | \mathbf{d})) + \sum_{l=1}^L \log |\det \mathbf{J}_l(\mathbf{x}_l | \mathbf{d})|$, where L is the total number of transformation layers in the CNF. The Jacobian, \mathbf{J}_l , of each layer l is a function of the input \mathbf{x}_l and the condition \mathbf{d} . Kang et al. [2022], Moon et al. [2023], Guan et al. [2023], Chen et al. [2025] use this conditioning concept for TSAD, all focusing on various levels of embedding creation of the temporal context for the definition of \mathbf{d} .

3 Proposed Methodology

In this section, we present a time-series probabilistic framework suited for anomaly detection, based on a discrete-time state-space model that captures the temporal evolution of the data according to prescribed inductive biases. In line with Li et al. [2025], we argue that structural inductive biases are required for a model to know what constitutes *unexpected behavior* solely from maximizing likelihood on samples with *expected behavior*.

We propose not only to (i) shift the AD mechanism from the ambient to the semantic latent space, but also to (ii) enforce inductive biases in such latent space, to capture the *expected behavior manifold*. For the former, we use CNFs for the observation- to latent-space mapping. For the latter, we prescribe expected dynamics over the latent representations’ evolution over time. Rather than modeling static distributions over data, we constrain the dynamics of the learned representations to evolve according to prescribed inductive biases.

Consequently, compliance with the inductive bias, i.e., the prescribed expected dynamics, serves as the definition of *expected behavior*:

- **Training-time compliance:** With sufficient model capacity and under model likelihood optimization, the imposed inductive bias determines the latent trajectories of observations, thereby defining which latent, temporal evolutions are *expected behavior*.
- **Testing-time compliance:** At inference time, the mapped representations of new observations should be similar to latent trajectories observed during training and consistent with the

prescribed latent distribution. Hence, an input sequence, after the non-linear observation-to latent-space mapping, is an anomaly if it does not comply with such *expected behavior*.

With this framework, we frame unsupervised time-series anomaly detection as a check for inductive bias compliance, rather than relying on model-based likelihood scores.

We proceed to describe in detail each of the components of the framework: the CNF-based state-space model with inductive bias in Section 3.1, along with its training procedure, and the time-series anomaly detection procedure as a check for inductive bias compliance in Section 3.2.

3.1 The probabilistic state-space model

We denote the sequence of observations with $\mathbf{x}_t \in \mathbb{R}^D$, indexed by time $t \in \mathbb{N}$, and introduce a corresponding latent state variable $\mathbf{z}_t \in \mathbb{R}^D$ to represent the underlying semantic dynamics of the system.

There are two key components to the proposed deep probabilistic model:

1. **A Conditional Normalizing Flow (CNF)**, parameterized by θ and with temporal context \mathbf{W} , mapping each observation \mathbf{x}_t into a latent representation \mathbf{z}_t , conditioned on a finite history of previous observations, $\mathbf{W}_t = \mathbf{x}_{t-k:t-1}$:

$$\mathbf{z}_t = F(\mathbf{x}_t | \mathbf{W}_t; \theta) \sim \mathcal{N}(\boldsymbol{\mu}_t, \boldsymbol{\Sigma}_t)^1. \quad (1)$$

2. **The Latent Dynamics**, imposing an explicit inductive bias on the temporal evolution of the latent representations, via deterministic dynamics of its mean:

$$\boldsymbol{\mu}_0 \sim p(\phi_0), \quad (2)$$

$$\boldsymbol{\mu}_t = \psi(\boldsymbol{\mu}_{t-1}; \phi). \quad (3)$$

The inductive bias, which constrains latent trajectories to follow a prescribed dynamical law, is defined in a generic form, as a deterministic dynamic map $\psi(\cdot|\phi)$.

Various inductive biases can be used within this general framework, depending on the specific application, prior problem knowledge, or other practical reasons. Next, we describe a simple inductive bias that is useful both for explainability and for anomaly detection.

3.1.1 The linear-Gaussian latent dynamical model (LG-LDM)

We can impose linear-Gaussian expected dynamics of the latent representation via

$$\boldsymbol{\mu}_0 \sim p(\phi_0) = \mathcal{N}(\mathbf{0}, \mathbf{I}), \quad (4)$$

$$\boldsymbol{\mu}_t = \psi(\boldsymbol{\mu}_{t-1}; \phi) = \mathbf{A}\boldsymbol{\mu}_{t-1} + \mathbf{b}, \quad (5)$$

with uncorrelated latent uncertainty, $\boldsymbol{\Sigma}_t = \mathbf{I}$, $\forall t$, where the learnable parameters for the LG-LDM are $\phi = \{\mathbf{A}, \mathbf{b}\}$. With such inductive bias, we impose a closed-form time-evolution for the expected representation $\boldsymbol{\mu}_t$ of the form

$$\boldsymbol{\mu}_t = \mathbf{A}^t \boldsymbol{\mu}_0 + \sum_{k=0}^{t-1} \mathbf{A}^k \mathbf{b}, \quad (6)$$

where \mathbf{A}^k is the k -th matrix power and the sum is a matrix–vector product at each time k .

If $\boldsymbol{\mu}_0 = \mathbf{0}$ and $\rho(\mathbf{A}) < 1$, then $\lim_{t \rightarrow \infty} \boldsymbol{\mu}_t = (\mathbf{I} - \mathbf{A})^{-1} \mathbf{b}$, by the matrix geometric series: i.e., the trajectory converges to a fixed point, and if $\mathbf{b} = \mathbf{0}$, then such a fixed point is the origin.

¹For any random variable $\mathbf{z}_t \sim \mathcal{N}(\boldsymbol{\mu}_t, \boldsymbol{\Sigma}_t)$ with known sufficient statistics $\boldsymbol{\mu}_t, \boldsymbol{\Sigma}_t$ we define its whitened counterpart $\tilde{\mathbf{z}}_t = \boldsymbol{\Sigma}_t^{-1/2}(\mathbf{z}_t - \boldsymbol{\mu}_t) \sim \mathcal{N}(\mathbf{0}, \mathbf{I})$.

3.1.2 Probabilistic training of the state-space model

The training procedure that aligns the CNF mapping of observations with the prescribed inductive bias, i.e., the latent dynamics, follows minimization of the negative log-likelihood (NLL) of the model. We jointly train the CNF parameters θ and the parameters of the latent dynamics ϕ via NLL optimization. The procedure ensures that the learned latent trajectories are consistent with the deterministic evolution encoded by $\psi(\cdot)$, both in their dynamics and its prescribed distribution.

Notably, the inductive bias-based DPM can be optimized either sequentially over the complete time-series or using sub-sequences over-time, with computational benefits. We present these below, with the choice depending on the computational resources of practitioners.

Training with complete time-series. We can sequentially train the CNF over the complete time-series via

$$\mathcal{L}_{seq}(\mathcal{D}) = -\frac{1}{T} \sum_{t=1}^T \left[\log p_t(\mathbf{F}(\mathbf{x}_t | \mathbf{W}_t)) + \sum_{l=1}^L \log |\det \mathbf{J}(\mathbf{F}_l)(\mathbf{x}_{t,l} | \mathbf{W}_t)| \right], \quad (7)$$

$$\text{with } p_t(\cdot) = \mathcal{N}(\boldsymbol{\mu}_t, \boldsymbol{\Sigma}_t), \quad (8)$$

$$\text{where } \boldsymbol{\mu}_0 \sim p(\phi_0), \boldsymbol{\mu}_t = \psi(\boldsymbol{\mu}_{t-1}; \phi). \quad (9)$$

Note that this training approach scales with T , as the optimization step of the loss depends on the full time-series.

Training with mini-batches of observations over time. Alternatively, for Markovian dynamics as in Eq. (3), a more computationally efficient approach is possible, where the NLL is computed for mini-batches over time.

We can split a time-series over B sub-sequences/mini-batches of size BS , i.e., $\mathbf{X}_b = \{\mathbf{x}_{bs}\}_{bs=1}^{BS}$, and write

$$\mathcal{L}_{batch}(\mathcal{D}) = -\frac{1}{B} \sum_{b=1}^B \frac{1}{BS} \left[\log p_b(\mathbf{F}(\mathbf{X}_b | \mathbf{W}_b)) + \sum_{l=1}^L \log |\det \mathbf{J}(\mathbf{F}_l)(\mathbf{X}_{b,l} | \mathbf{W}_b)| \right], \quad (10)$$

$$\text{with } p_b(\cdot) = \{\mathcal{N}(\boldsymbol{\mu}_{bs}, \boldsymbol{\Sigma}_{bs})\}_{bs=1}^{BS}, \quad (11)$$

where \mathbf{W}_b are the corresponding temporal contexts to each sample in the mini-batch, and $\boldsymbol{\mu}_0 \sim \mathcal{N}(\mathbf{0}, \mathbf{I})$ in mini-batch 1, and the last mean $\boldsymbol{\mu}_{bs}$ from the previous mini-batch $b-1$ is the initializing $\boldsymbol{\mu}_0$ for each consecutive mini-batch b .

In this mini-batched version of training, we can update model parameters after each mini-batch, and $\mathcal{L}_{batch}(\mathcal{D})$ reports the average loss over all mini-batches.

This is possible whenever we can pre-compute all the necessary expected representations for each mini-batch of the input time-series, as we can then split the observations of a time-series over time into subsequences/mini-batches, reducing the computational dependency on the time-series length T . Obviously, when $BS = T$, and $B = 1$, we recover the full sequential version.

3.2 Latent dynamic compliance as a statistical test

In our probabilistic framework, the prescribed inductive bias is reflected in the learned latent dynamics. Therefore, compliance of observations with such inductive bias and unsupervised anomaly detection are two-sides of the same coin: *expected and unexpected behavior* are nothing but *compliance and non-compliance* with the inductive bias.

Because the inductive bias in Equations 2- 3 enforces distributional constraints on latent trajectories, learned representation compliance can be measured via a goodness-of-fit (GOF) test between the prescribed evolving distribution and the empirical distribution of the mapped trajectories.

In what follows, we use the multivariate Kolmogorov-Smirnov (MV-KS) GOF test to quantify compliance, due to its generality, its non-parametric nature, and its exactness even under small sample sizes [Naaman, 2021]. The MV-KS test quantifies GOF to a prescribed distribution, providing the KS statistic (s) and a critical value (τ) for decision-making: we can reject that samples come from the prescribed distribution if the KS statistic is bigger than the critical value, i.e., $s \geq \tau$. The MV-KS critical value is non-parametric and dependent on the sample size.

Compliance to inductive bias: successful learning. We expect and require that a well-trained CNF model maps observations of *expected behavior* into latent dynamics that comply with the inductive bias. Therefore, the result of a GOF test indicates whether the trained model is compliant with the prescribed dynamics. Due to its non-parametric definition and sample-size adaptability, the MV-KS statistic computed on latent training trajectories provides a data-driven notion of expected behavior, i.e., it measures how compliant latent representations are, bypassing the need for threshold tuning. Note that such statistic computed in the training data is an automatic, model training diagnostic metric: good model learning will enforce latent representations to obey prescribed latent distribution dynamics —see an illustrative example in Fig. 3, where for the LG-LDM, the inductive bias prescribes standard Gaussian representations, whitened over time, to which latent trajectories comply.

Non-compliance to inductive bias: anomaly detection. On the contrary, we can identify *unexpected behavior* by checking whether an input sequence, after the non-linear observation- to latent-transformation by the CNF, follows or not the expected dynamics, as determined by a GOF test.

Specifically, for the MV-KS test, we can flag a sequence of observations as anomalies according to

$$H(s) = \begin{cases} \text{expected behavior,} & \text{if } s < \tau \\ \text{unexpected behavior,} & \text{otherwise.} \end{cases} \quad (12)$$

Notice how, within this unsupervised AD framework based on MV-KS tests, no manual AD threshold needs to be defined. Namely, the CNF trained according to available data determines the operating point for anomaly detection.

4 Evaluation

We assess the proposed framework for anomaly detection on synthetic and real-world data by enforcing linear dynamics in the latent space, i.e., the LG-LDM inductive bias in Section 3.1.1. We first describe our experimental setup, including the hyperparameter optimization strategy and the reported metrics. We then study synthetic data to demonstrate the limitations of standard likelihood-based AD and illustrate the benefits of the proposed framework. Finally, we compare our method against baselines on real-world data to assess its sensitivity and performance.

4.1 Experimental Setup

Our framework is optimized using the NLL presented in Section 3.1.2, which jointly optimizes the CNF and, in this case, the LG-LDM parameters. For the CNF, we use a variant of the RealNVP architecture, originally proposed by Dinh et al. [2017] and extended by Rasul et al. [2020].

We evaluate our framework on synthetic and real data. In the synthetic data experiments, we assess the performance across a range of frequency, amplitude, and noise changes as sequence anomalies (Fig. 2). On the real-world data, we evaluate and compare performance on a subset of univariate² and multivariate real-world sequences (TSB-AD) [Liu and Paparrizos, 2024]. Although we calculate all metrics based on TSB-AD’s implementation, we can only compare results in detail on the *Volume Under the Surface Precision-Recall* (VUS-PR) curve. This is because per-sequence results are publicly available only for this metric. We select a fair set of statistics and deep learning methods from TSB-AD as baselines, based on their rankings, as reported in [Liu and Paparrizos, 2024]. We also report aggregated, oracle-thresholded results on NLL & KS for the proposed AD in Section B.1 and Section B.2.

²Univariate series are duplicated to adapt to the default multivariate interface of our framework.

Table 1: Overview of the hyperparameters and their search ranges. The hyperparameters refer to different parts of our framework, such as the LG-LDM (D), the CNF (C), or the implementation (S). “NA” stands for sequential training.

	Parameter	Synthetic	Real-world
D	Learning \mathbf{b}	[True, False]	True
C	Temporal Context	[20, 40, 100]	5 to 500
C	CNF layers	[6, 8, 12]	3 to 40
C	Hidden layers	[1, 3]	1 to 20
C	Hidden layer size	[64, 128]	4 to 200
S	Batch size	[NA, 2048]	2048

For model hyperparameter tuning, we use a grid search for synthetic data and Optuna [Akiba et al., 2019] (TPE; 20 warm-up + 100 trials) for TSB-AD data. The hyperparameters and their evaluated ranges are listed in Table 1. Code, models, and tables are available in a GitHub repository ³.

4.2 Experimental Results

Model Negative log-likelihood Vs inductive bias compliance. We present in Fig. 1 an example time-series with amplitude and frequency anomalies blended in —see shaded background areas and original training data with dashed lines. Table 2 contains the metric results for this model and experiment, comparing AD performance based on the raw NLL score and the proposed MV-KS alternative.

The results highlight the limitations of NLL-based scoring, as it is only able to detect the first anomaly around $t = 200$. Frequency-based modifications within the sequence are flagged by both scores, but for amplitude-based anomalies, only the MV-KS-based AD identifies the anomalies around $t = 500$ and $t = 800$. This occurs because the CNF tends to place these input-data points into high-density latent regions. However, even in these high-likelihood, representation space regions, these trajectories do not obey *expected behavior*. Hence, as we test \tilde{z}_t compliance via MV-KS tests, its score —as shown by the heatmaps in Fig. 1— reveals unexpected behavior around all three anomaly sequences.

We further investigate the proposed unsupervised AD methodology’s robustness to different anomalies, by assessing how sensitive the MV-KS test is to variations in amplitude, frequency and observation noise with respect to the training time-series. Figure 2 summarizes the methodology’s performance, showcasing the MV-KS score-difference between the training sequence and the modified time-series, as well as the interpretable representation space for a subset of selected cases. The latent, whitened \tilde{z}_t space is compliant with the LG-LDM inductive bias only on training data, i.e., Gaussian shape samples with $KS = 0.02$; while it showcases visually noticeable departures (a doughnut shape, stretched and enlarged samples) for minor and major test-set deviations. Even sequences with a minor change in frequency and amplitude, that result in a visually subtle difference, are flagged by the MV-KS test: $s = 0.076 > 0.02$, $\tau = 0.075$.

Anomaly Detection via MV-KS tests: the impact of window size. A key AD design choice is what window-size to use to determine whether a time-series subsequence is an anomaly or not. In our case, this window size is directly related to the statistical power of the GOF test, as it determines the length of the latent trajectory and, hence, the number of samples used. Specifically, the MV-KS test depends on the number of samples available to compute reliable statistics. As shown in Fig. 1, window sizes of $w \leq 20$ are usually too noisy to separate anomalous from compliant distributions in 4-dimensional time-series, while $w \geq 200$ dilutes the identified anomalies, degrading computed metrics. We report corresponding AD metrics for different window sizes in Table 2. In general, we recommend a window size of $\mathcal{O}(D^3)$, which matches the empirical sweet spot for $w = 64$ in this experiment: window size $w = 64$ achieves AUC-PR 82.1 and VUS-PR 96.0, in comparison with NLL-based performance of 78.8 and 92.8, respectively. Large gains are also observed in ranged-F1 (65.5 vs. 36.0) and affiliation F1 (92.6 vs. 85.0) scores.

³<https://anonymous.4open.science/r/latent-inductive-flows-3422>

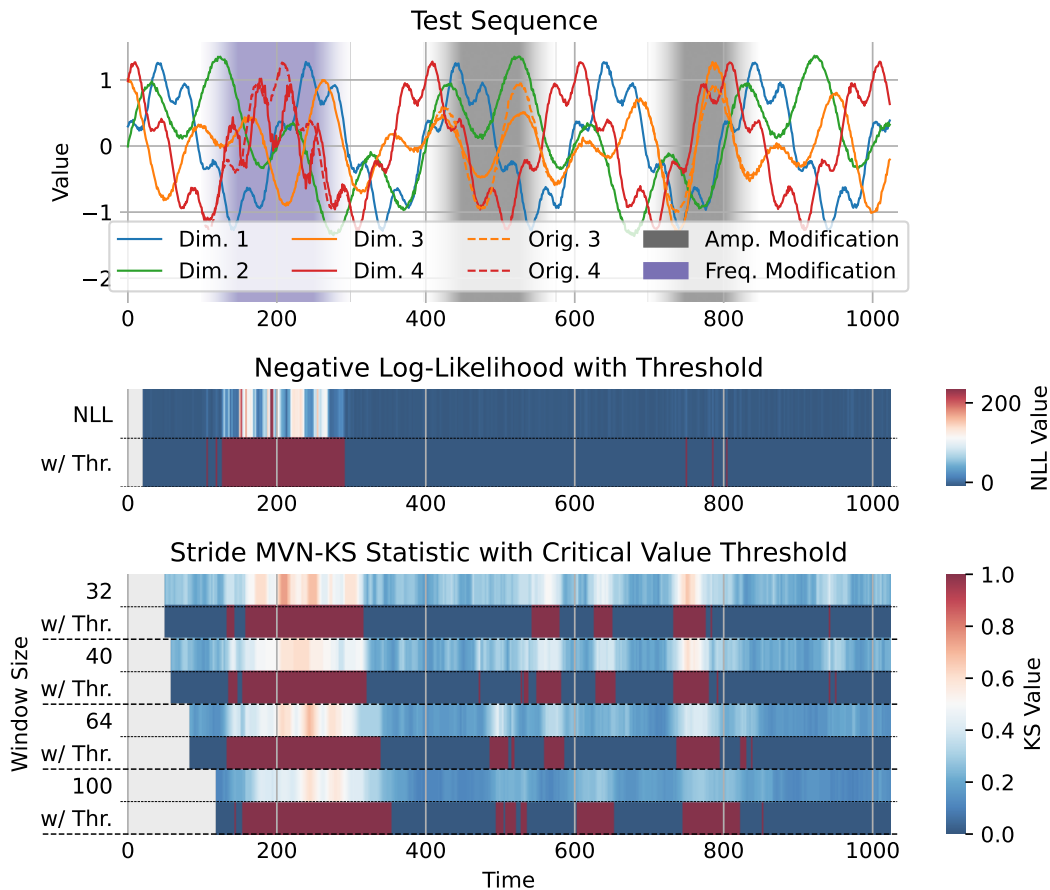


Figure 1: Anomaly detection comparison between the proposed moel when using NLL scores and proposed GOF test. (Top) The input sequence, contaminated with amplitude and frequency modifications (in shared regions). (Middle) Heatmap of the continuous and thresholded NLL (threshold set to the maximum NLL value in training): NLL-based scores fail to detect amplitude changes. (Bottom) The MV-KS score heatmap, showing successful detection of the modified sections. As detailed in Table 2, our approach outperforms the NLL baseline across various metrics, highlighted by a 7% improvement in the affiliation F1 score.

Table 2: Non-parametric MV-KS results for the test case in Fig. 1. Parametric results covering NLL and MV-KS w/wo critical value (CV) thresholding or the AUC-ROC curve as threshold for scoring, are in Section A.

Score Source	AUC		VUS	
	PR	ROC	PR	ROC
NLL	78.8	70.9	92.8	90.9
KS w=20	79.9	71.9	92.4	90.4
KS w=32	79.1	72.8	93.8	92.0
KS w=40	80.1	73.0	94.6	92.8
KS w=64	82.1	73.1	96.0	93.7
KS w=100	74.5	66.3	92.7	91.1
KS w=200	58.3	64.8	90.4	92.2
KS w=400	78.3	69.1	89.5	86.9

Training diagnostics via inductive bias compliance. As discussed in Section 3.2, we can test inductive bias compliance, and hence good model learning, by MV-KS testing training trajectories mapped onto \tilde{z}_t . If for most training subsequences mapped onto \tilde{z}_t , a MV-KS score below the

MVN-KS Difference to Training Based on Changed Sequence Parameters

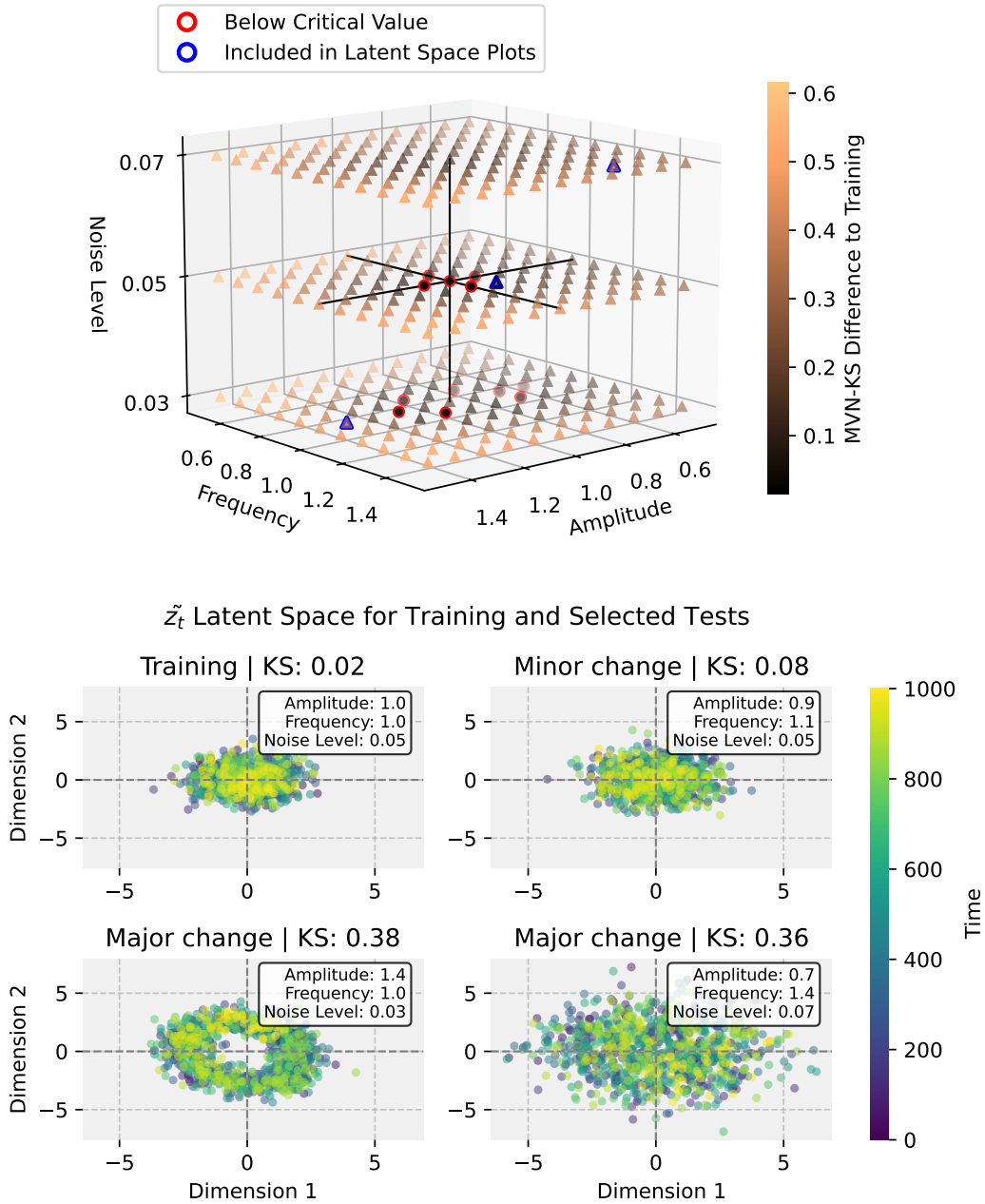


Figure 2: Sensitivity of the latent space GOF to input data variations. (3D Plot) The test range, where the color gradient encodes the relative difference in MVN-KS values compared to the baseline training sequence at the center. Points with a red border remain below the critical threshold, despite having higher MVN-KS values than the training baseline. (2x2 Scatter Plot) Visualizes the z_t latent space for the training sequence and three modified test cases (blue borders). Overall, the reported MVN-KS values indicate that greater deviations from the training sequences lead to more pronounced violations of the GOF criteria.

critical value is attained, we can conclude that the inductive bias is well-prescribed. We can therefore be confident that the model is well-trained and ready for AD detection: the MV-KS critical value is a valid, unsupervised threshold.

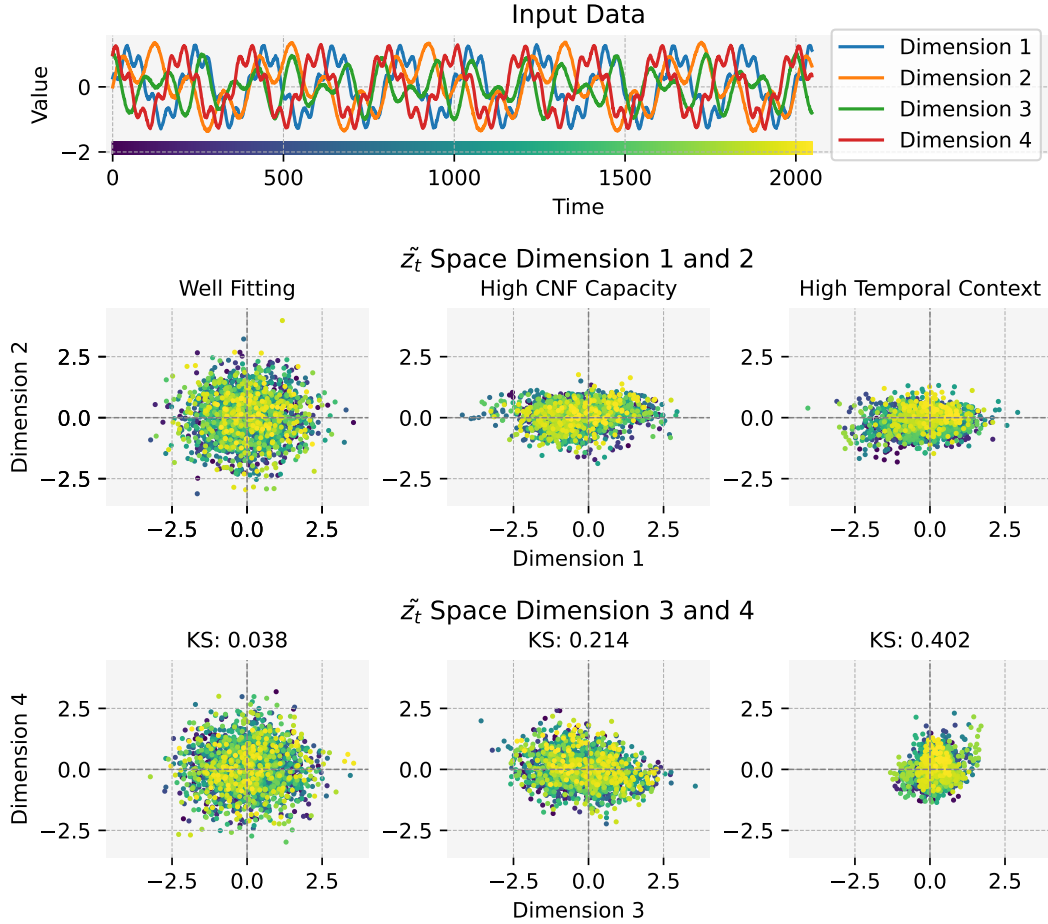


Figure 3: Example of 3 different CNF configurations and their impact on the \tilde{z}_t latent space. The first column shows a well-fitting and trustworthy model. The remaining columns show two models with too many layers or too much temporal context. A version including the μ_t space is in Section B.3.

In Fig. 3, we present a comparison of 3 CNF variants, one per column, where we can visually (and through MV-KS scores) assess compliance with inductive bias. In the left column, we observe the latent state of a well-trained model, with very low $KS = 0.038$ score. In contrast, in the other two columns, we observe how \tilde{z}_t trajectories deviate systematically from the (in this case, Gaussian) inductive bias. Due to excessive CNF capacity, mismatched context length, or data complexity, training data are not compliant, invalidating the automatic KS-based threshold. This training diagnostic, where we can quantify the fraction of sequences passing the MV-KS test, is useful for real-world data —see the *FIT* column in Table 3— as it directly predicts when the trained model and its MV-KS score can be trusted for AD.

Training compliance for unsupervised VS. oracle-based thresholding. We assess the value of the above-mentioned training compliance diagnostic with real-world data, as reported in Table 8. When compliance to inductive bias is met (see *FIT* column in table), the label-free, unsupervised MV-KS critical value-based AD performs close to the oracle-based, thresholded KS score in the Affiliation F1 metric. When anomaly labels are available, the oracle-thresholded NLL score is a strong competitor on the VUS-PR metric. We acknowledge that KS performs worse than the NLL version on the tested real-world sequences. We hypothesize that this might be due to the type of anomalies in these datasets, since NLL scores can have shortcomings as shown in the synthetic experiments. Additionally, we emphasize that we advocate for the MV-KS score for unsupervised AD, which does not require labels or thresholding.

AD in real-world benchmark data. We report AD performance across a variety of metrics in Tables 3 and 4. In general, we achieve competitive (better, or in par) results than baselines, even when model learning is not fully compliant with the LG-LDM inductive bias. When compliance is successful, e.g., on 88% of sequences in NEK and 100% in the Stock datasets, the NLL approach performs in the top-2, with MV-KS following close, specially on the VUS-PR metric for univariate datasets. In the multivariate setting Table 4), both NLL and MV-KS are competitive. On the MITDB dataset, the imposed latent dynamics are not realized after our training, and, as predicted, both scoring rules underperform.

Table 3: Aggregated univariate sequence results on the VUS-PR metric with mean and standard deviation results. Comparative results from TSB-AD are included, and a complete table is in the appendix.

Set	Sub-PCA	CNN	IForest	FITS	AutoEncoder	TimesNet	CNF & LG-LDM		
							NLL	KS	FIT
IOPS	22.7 ± 20	26.0 ± 20	27.7 ± 15	17.3 ± 15	25.5 ± 22	22.4 ± 21	33.5 ± 24	18.7 ± 13	13%
MITDB	36.3 ± 32	15.3 ± 13	9.8 ± 6	9.0 ± 7	7.4 ± 4	8.4 ± 5	19.3 ± 13	16.3 ± 9	0%
NEK	90.5 ± 14	73.5 ± 22	59.3 ± 14	49.4 ± 25	50.6 ± 34	37.4 ± 26	73.7 ± 25	70.0 ± 34	88%
Stock	84.0 ± 15	92.2 ± 17	99.3 ± 1	76.3 ± 28	72.0 ± 28	78.8 ± 27	93.9 ± 9	81.9 ± 17	100%
TODS	53.9 ± 24	54.3 ± 26	51.8 ± 30	58.1 ± 19	65.2 ± 11	58.6 ± 20	60.3 ± 25	48.5 ± 27	85%

Table 4: Aggregated multivariate sequences results on the VUS-PR metric with mean and standard deviation results. Comparative results from TSB-AD are included, and a complete table is in the appendix.

Set	PCA	CNN	FITS	TimesNet	OmniAnomaly	CNF & LG-LDM		
						NLL	KS	FIT
LTDB	24.4 ± 18	32.8 ± 25	22.8 ± 18	27.2 ± 23	44.4 ± 38	35.0 ± 20	33.9 ± 21	25%
MITDB	6.5 ± 6	14.0 ± 16	5.3 ± 6	6.8 ± 7	11.5 ± 11	15.2 ± 15	12.3 ± 9	18%

5 Discussion

The evaluation of the proposed framework—with the specific implementation of a CNF with an LG-LDM that constrains time-series representations to temporally coherent whitened Gaussian trajectories—demonstrates its value, interpretability and robustness for unsupervised anomaly detection.

As shown in Figures 1-2, checking inductive bias compliance (via GOF-tests) of incoming observations, after mapping them to the latent space via the trained CNF, provides an interpretable (visual) and robust (MV-KS) method to identify *unexpected behavior* for it to be flagged as an anomaly.

We emphasize that the proposed method enables AD even in high-density areas of the trained model (see Figure 1) due to our use of (i) inductive bias in the latent representations—that impose time-evolving distributional constraints—and (ii) statistical GOF tests over these latent trajectories. That is, incoming observations might be mapped to a clustered or structured latent region of the model, which are often not directly detectable via NLL-based scoring [Morningstar et al., 2021, Li et al., 2025]. However, even if they are located in a high-density area of our trained CNF, it is by checking compliance with the prescribed inductive bias (the LG-LTM time-varying dynamics in our experiments) that we can successfully detect *unexpected behavior*.

We acknowledge that, because latent dynamic compliance relies on statistical GOF testing against the prescribed inductive bias, its efficacy is inherently dependent on the chosen test statistic and the available sample size. This dependency is particularly sensitive in high-dimensional spaces, where statistical tests frequently suffer from low power due to the curse of dimensionality [Bing and Latremouille, 2025, Chen and Xia, 2023, Morningstar et al., 2021]. Hence, our approach may require large temporal windows that can smooth over and hide isolated point anomalies.

To mitigate this effect, we recommend scaling the MV-KS window size by the latent dimension D , with a recommended minimum of $\mathcal{O}(D^3)$. A computationally cheaper alternative is to rely on subspace GOF testing: if the imposed inductive bias allows it, e.g., factorized latent Gaussianity,

one may perform tests on lower-dimensional subspaces of the full latent representations. This reduces the sample complexity required for each test, although it relies on multiple-testing, and the limitations of compliance checking via marginal distributions.

A final limitation worth discussing is that the proposed framework is highly sensitive to model capacity and to specific dataset behaviors. For the former, we recommend thorough hyper-parameter searches, see Section 4.1. For the latter, expert knowledge is highly valuable, both for pre-processing of the input data and for definition of the inductive bias: e.g., the LG-LDM is not a suitable inductive bias for all real-world datasets. In any case, we suggest relying on the monitoring of the training procedure via GOF test-based inductive bias compliance as described in Section 3.2 and showcased empirically in Figure 3.

6 Conclusions

We introduced a state-space, deep generative model with latent-space inductive bias for unsupervised time-series anomaly detection. Specifically, we proposed a label-free anomaly detector that scores latent dynamic compliance via GOF tests of representations learned by a CNF, eliminating the need for manual threshold tuning. Crucially, our framework provides a practical model learning diagnostic that builds upon the explicit inductive bias: we apply a GOF test to the mapped training time-series to verify whether the imposed inductive bias is well-prescribed and realized by the learned model. Consequently, the GOF critical-value decision rule becomes valid and trustworthy for AD deployment. This principled decision rule remains effective even in regions of high observation likelihood.

Presented results support a broader, unifying perspective on deep generative anomaly detection, demonstrated by experiments on synthetic and real-world time-series. Rather than relying on model likelihood as a proxy for expected data behavior, anomaly detection can be effectively framed as testing whether learned representations satisfy an explicit, application-motivated inductive bias over-time.

While the method shows good performance in identifying unexpected behavior without labels, its limitations regarding adapting the model to the data and the multivariate GOF test’s limitations suggest several avenues for further investigation. Future work will focus on learning other inductive bias over-time: e.g., learnable LG-LDM covariance matrix, non-Markovian LG-LDMs, or non-linear models. Additional avenues for exploration are assessing the impact of MVN-KS window alignment, extending the framework to other data types, exploring its generative capabilities, and developing data-space explanations of unexpected behavior to complement our latent-space diagnostics.

Acknowledgements

This work has been partly funded by the SFI NorwAI, (Centre for Research-based Innovation, 309834). B. Baumgartner, thanks the financial support from the Research Council of Norway and the partners of the SFI NorwAI. E. da Silva. and I. Urteaga thank the support of “la Caixa” foundation’s LCF/BQ/PI22/11910028 award, as well as the Basque Government through the BERC 2022-2025 program and the Ministry of Science and Innovation: BCAM Severo Ochoa accreditation CEX2021-001142-S/MICIN/AEI/10.13039/501100011033. I. Urteaga is also partially supported by Grant RYC2023-045922-I funded by MICIU/AEI/10.13039/501100011033 and by ESF+, We sincerely appreciate the valuable comments and suggestions from Melissa Yan and Heri Ramampiaro, which helped us improve the quality of the manuscript.

References

- Takuya Akiba, Shotaro Sano, Toshihiko Yanase, Takeru Ohta, and Masanori Koyama. Optuna: a next-generation hyperparameter optimization framework. In *Proceedings of the 25th ACM SIGKDD International Conference on Knowledge Discovery & Data Mining, KDD '19*, pages 2623–2631, New York, NY, USA, July 2019. Association for Computing Machinery. ISBN 978-1-4503-6201-6. URL <https://dl.acm.org/doi/10.1145/3292500.3330701>.
- Julien Audibert, Pietro Michiardi, Frédéric Guyard, Sébastien Marti, and Maria A. Zuluaga. USAD: UnSupervised anomaly detection on multivariate time series. In *Proceedings of the 26th ACM*

- SIGKDD International Conference on Knowledge Discovery & Data Mining, KDD '20*, New York, NY, USA, August 2020. Association for Computing Machinery. ISBN 978-1-4503-7998-4. URL <https://dl.acm.org/doi/10.1145/3394486.3403392>.
- Kamal Berahmand, Fatemeh Daneshfar, Elaheh Sadat Salehi, Yuefeng Li, and Yue Xu. Autoencoders and their applications in machine learning: a survey. *Artificial Intelligence Review*, 57(2):28, February 2024. ISSN 1573-7462. URL <https://doi.org/10.1007/s10462-023-10662-6>.
- Xin Bing and Derek Latremouille. High-dimensional invariant tests of multivariate normality based on radial concentration, April 2025. URL <https://arxiv.org/abs/2504.09237v2>.
- Varun Chandola, Arindam Banerjee, and Vipin Kumar. Anomaly detection: a survey. *ACM Computing Surveys*, 41(3):15:1–15:58, July 2009. ISSN 0360-0300. URL <https://doi.org/10.1145/1541880.1541882>.
- Hao Chen and Yin Xia. A normality test for high-dimensional data based on the nearest neighbor approach. *Journal of the American Statistical Association*, 118(541):719–731, January 2023. ISSN 0162-1459. URL <https://doi.org/10.1080/01621459.2021.1953507>.
- Kun Chen, Jianmin Xiao, Quan Liu, Ziling Huang, Chao Ji, and Kehuai Ji. Robust multivariate time series anomaly detection via conditional normalizing flow with patch embedding and cross time attention. *Autonomous Transportation Research*, December 2025. ISSN 3050-8622. URL <https://doi.org/10.1016/j.atres.2025.12.001>.
- Laurent Dinh, Jascha Sohl-Dickstein, and Samy Bengio. Density estimation using real NVP. In *International Conference on Learning Representations*, 2017. URL <https://openreview.net/forum?id=HkpbhH91x>.
- Alexander Geiger, Dongyu Liu, Sarah Alnegheimish, Alfredo Cuesta-Infante, and Kalyan Veeramachaneni. TadGAN: time series anomaly detection using generative adversarial networks. pages 33–43. IEEE Computer Society, December 2020. ISBN 978-1-7281-6251-5. URL <https://doi.org/10.1109/BigData50022.2020.9378139>.
- Ian J. Goodfellow, Jean Pouget-Abadie, Mehdi Mirza, Bing Xu, David Warde-Farley, Sherjil Ozair, Aaron Courville, and Yoshua Bengio. Generative adversarial nets. In *Advances in Neural Information Processing Systems*, volume 27. Curran Associates, Inc., 2014. URL <https://dl.acm.org/doi/10.5555/2969033.2969125>.
- Siwei Guan, Zhiwei He, Shenhui Ma, and Mingyu Gao. Conditional normalizing flow for multivariate time series anomaly detection. *ISA Transactions*, 143:231–243, December 2023. ISSN 0019-0578. URL <https://doi.org/10.1016/j.isatra.2023.09.002>.
- Zhuangwei Kang, Ayan Mukhopadhyay, Aniruddha Gokhale, Shijie Wen, and Abhishek Dubey. Traffic anomaly detection via conditional normalizing flow. In *2022 IEEE 25th International Conference on Intelligent Transportation Systems (ITSC)*, pages 2563–2570, October 2022. URL <https://doi.org/10.1109/ITSC55140.2022.9922061>.
- Diederik P. Kingma and Max Welling. Auto-encoding variational bayes, December 2022. URL <http://doi.org/10.48550/arXiv.1312.6114>.
- Yucen Lily Li, Daohan Lu, Polina Kirichenko, Shikai Qiu, Tim G. J. Rudner, C. Bayan Bruss, and Andrew Gordon Wilson. Position: Supervised Classifiers Answer the Wrong Questions for OOD Detection. June 2025. URL <https://openreview.net/forum?id=UXZJ3aL8vE>.
- Qinghua Liu and John Paparrizos. The elephant in the room: towards a reliable time-series anomaly detection benchmark. *Advances in Neural Information Processing Systems*, 37:108231–108261, December 2024. URL <https://doi.org/10.52202/079017-3437>.
- Jiwon Moon, Seunghwan Song, and Jun-Geol Baek. Multivariate time series anomaly detection via temporal encoder with normalizing flow. In *2023 International Conference on Artificial Intelligence in Information and Communication (ICAIC)*, pages 620–624, February 2023. URL <https://doi.org/10.1109/ICAIC57133.2023.10067087>.

- Warren Morningstar, Cusuh Ham, Andrew Gallagher, Balaji Lakshminarayanan, Alex Alemi, and Joshua Dillon. Density of States Estimation for Out of Distribution Detection. In *Proceedings of The 24th International Conference on Artificial Intelligence and Statistics*, pages 3232–3240. PMLR, March 2021. URL <https://proceedings.mlr.press/v130/morningstar21a.html>.
- Michael Naaman. On the tight constant in the multivariate dvoretzky–kiefer–wolfowitz inequality. *Statistics & Probability Letters*, 173:109088, June 2021. ISSN 0167-7152. URL <https://doi.org/10.1016/j.spl.2021.109088>.
- Guansong Pang, Chunhua Shen, Longbing Cao, and Anton Van Den Hengel. Deep learning for anomaly detection: a review. *ACM Comput. Surv.*, 54(2):38:1–38:38, March 2021. ISSN 0360-0300. URL <https://dl.acm.org/doi/10.1145/3439950>.
- George Papamakarios, Eric Nalisnick, Danilo Jimenez Rezende, Shakir Mohamed, and Balaji Lakshminarayanan. Normalizing flows for probabilistic modeling and inference. *Journal of Machine Learning Research*, 22(1):57:2617–57:2680, 2021. ISSN 1532-4435. URL <http://jmlr.org/papers/v22/19-1028.html>.
- Marco A. F. Pimentel, David A. Clifton, Lei Clifton, and Lionel Tarassenko. A review of novelty detection. *Signal Processing*, 99:215–249, June 2014. ISSN 0165-1684. URL <https://doi.org/10.1016/j.sigpro.2013.12.026>.
- Kashif Rasul, Abdul-Saboor Sheikh, Ingmar Schuster, Urs M. Bergmann, and Roland Vollgraf. Multivariate probabilistic time series forecasting via conditioned normalizing flows. In *International Conference on Learning Representations*, October 2020. URL <https://openreview.net/forum?id=WiGQBFuVRv>.
- Lukas Ruff, Jacob R. Kauffmann, Robert A. Vandermeulen, Grégoire Montavon, Wojciech Samek, Marius Kloft, Thomas G. Dietterich, and Klaus-Robert Müller. A unifying review of deep and shallow anomaly detection. *Proceedings of the IEEE*, 109(5):756–795, May 2021. ISSN 1558-2256. URL <https://doi.org/10.1109/JPR0C.2021.3052449>.
- Sebastian Schmidl, Phillip Wenig, and Thorsten Papenbrock. Anomaly detection in time series: a comprehensive evaluation. *Proceedings of the VLDB Endowment*, 15(9):1779–1797, 2022. ISSN 2150-8097. URL <https://doi.org/10.14778/3538598.3538602>.
- Joan Serrà, David Álvarez, Vicenç Gómez, Olga Slizovskaia, José F. Núñez, and Jordi Luque. Input Complexity and Out-of-distribution Detection with Likelihood-based Generative Models. September 2019. URL <https://openreview.net/forum?id=SyxIWpVYvr>.
- Sondre Sørnbø and Massimiliano Ruocco. Navigating the metric maze: a taxonomy of evaluation metrics for anomaly detection in time series. *Data Mining and Knowledge Discovery*, 38(3):1027–1068, May 2024. ISSN 1573-756X. URL <https://doi.org/10.1007/s10618-023-00988-8>.
- Xuan Xia, Xizhou Pan, Nan Li, Xing He, Lin Ma, Xiaoguang Zhang, and Ning Ding. GAN-based anomaly detection: a review. *Neurocomputing*, 493:497–535, July 2022. ISSN 0925-2312. URL <https://doi.org/10.1016/j.neucom.2021.12.093>.
- Haowen Xu, Wenxiao Chen, Nengwen Zhao, Zeyan Li, Jiahao Bu, Zhihan Li, Ying Liu, Youjian Zhao, Dan Pei, Yang Feng, Jie Chen, Zhaogang Wang, and Honglin Qiao. Unsupervised anomaly detection via variational auto-encoder for seasonal KPIs in web applications. In *Proceedings of the 2018 World Wide Web Conference, WWW '18*, pages 187–196, Republic and Canton of Geneva, CHE, April 2018. International World Wide Web Conferences Steering Committee. ISBN 978-1-4503-5639-8. URL <https://dl.acm.org/doi/10.1145/3178876.3185996>.
- Lily Zhang, Mark Goldstein, and Rajesh Ranganath. Understanding failures in out-of-distribution detection with deep generative models. In *Proceedings of the 38th International Conference on Machine Learning*, pages 12427–12436. PMLR, July 2021. URL <https://proceedings.mlr.press/v139/zhang21g.html>.

A Parametric results for synthetic case

Table 5: Various parametric F1 metric scores based on NLL and MVN-KS w/o critical value (CV) thresholding or the AUC-ROC curve as threshold on different window sizes for the test case in Fig. 1. Table 2 contains the non-parametric scores for NLL and MVN-KS.

Score Source	Standard F1	Point-adjusted F1	Event-based F1	Range-based F1	Affiliation F1
NLL	68.9	98.0	95.3	36.0	85.0
KS w=20	70.9	100.0	100.0	62.2	88.1
KS w=20 (CV)	55.0	97.1	93.2	46.7	86.9
KS w=32	71.0	99.2	96.7	57.1	89.2
KS w=32 (CV)	57.7	95.7	90.8	48.7	87.2
KS w=40	72.5	98.5	95.2	51.4	92.4
KS w=40 (CV)	60.1	94.9	89.8	43.7	87.7
KS w=64	72.0	99.5	98.3	65.5	92.6
KS w=64 (CV)	66.0	95.4	91.8	63.3	91.9
KS w=100	72.6	94.6	85.8	62.1	82.5
KS w=100 (CV)	59.3	90.4	83.0	56.2	80.9
KS w=200	70.4	89.0	80.6	73.6	85.2
KS w=200 (CV)	60.1	88.2	80.2	70.6	81.8
KS w=400	68.8	82.1	74.1	73.2	82.0
KS w=400 (CV)	60.8	60.8	60.1	35.5	64.9

B Results per sequence and aggregated

B.1 Additional Univariate Sequences Results

Table 6: Per-sequence univariate sequence results for the VUS-PR metric. It also includes in the FIT column whether the selected model meets the trustworthiness criteria.

Sequence	Sub-PCA	CNN	IForest	FITS	AutoEncoder	TimesNet	CNF & LG-LDM		
							NLL	KS	FIT
Stock, Id: 1	86.07	99.83	<u>99.5</u>	82.19	74.11	85.54	96.95	89.64	True
Stock, Id: 3	85.97	91.85	99.5	85.38	65.43	85.97	<u>94.29</u>	85.12	True
Stock, Id: 7	92.57	96.34	<u>99.7</u>	91.32	85.91	93.02	99.72	91.56	True
Stock, Id: 8	50.48	<u>50.47</u>	98.3	13.63	12.41	15.62	<u>71.19</u>	45.12	True
Stock, Id: 12	75.48	99.57	<u>98.99</u>	61.46	57.58	72.68	93.35	70.96	True
Stock, Id: 14	94.99	<u>99.73</u>	99.84	94.07	94.96	94.26	98.99	93.71	True
Stock, Id: 17	97.29	99.93	<u>99.82</u>	96.97	97.46	97.10	<u>99.9</u>	97.53	True
Stock, Id: 18	88.96	99.92	<u>98.77</u>	85.06	87.99	86.08	96.44	81.92	True
MITDB, Id: 1	8.85	6.57	6.74	6.24	5.35	6.70	<u>9.12</u>	10.96	False
MITDB, Id: 2	72.87	39.63	15.25	9.94	8.64	11.65	<u>41.32</u>	24.29	False
MITDB, Id: 3	1.84	7.66	2.55	2.40	3.38	2.39	15.17	<u>12.54</u>	False
MITDB, Id: 4	19.66	<u>17.82</u>	16.60	11.43	10.45	11.88	16.41	17.05	False
MITDB, Id: 6	25.14	3.79	3.89	3.63	3.68	3.45	<u>5.98</u>	5.63	False
MITDB, Id: 7	86.16	23.64	16.48	23.00	15.23	15.97	<u>32.79</u>	31.26	False
MITDB, Id: 8	39.43	7.76	7.04	6.43	5.22	6.49	<u>14.31</u>	12.45	False
IOPS, Id: 1	<u>22.62</u>	12.09	16.49	2.15	19.90	20.31	14.47	22.82	False
IOPS, Id: 2	1.18	<u>15.62</u>	10.76	8.07	40.27	12.61	8.66	2.81	False
IOPS, Id: 3	25.23	15.45	<u>30.6</u>	10.25	2.92	11.97	34.03	8.25	False
IOPS, Id: 4	10.61	67.83	13.42	46.94	<u>58.14</u>	41.61	35.45	10.01	False
IOPS, Id: 5	4.43	5.27	3.11	7.60	77.97	4.09	5.27	16.68	False
IOPS, Id: 7	62.01	4.35	<u>51.42</u>	2.70	4.78	5.75	37.58	15.88	False
IOPS, Id: 8	20.65	<u>37.96</u>	39.0	23.12	7.08	17.54	17.17	6.73	False
IOPS, Id: 9	23.63	16.59	<u>31.36</u>	17.92	13.44	15.94	52.08	20.37	False
IOPS, Id: 10	72.2	38.45	43.96	4.24	3.05	9.32	<u>70.03</u>	41.79	True
IOPS, Id: 12	14.59	15.36	27.12	17.45	<u>18.63</u>	14.33	8.65	10.91	True
IOPS, Id: 13	15.77	<u>69.18</u>	22.15	48.85	53.62	87.64	52.19	20.24	False
IOPS, Id: 14	4.42	<u>23.3</u>	9.59	7.26	13.55	33.09	5.51	2.08	False
IOPS, Id: 15	21.17	32.11	34.96	<u>35.61</u>	26.61	33.94	54.78	22.47	False
IOPS, Id: 16	9.47	16.34	32.76	12.32	24.65	13.31	30.03	<u>31.36</u>	False
IOPS, Id: 17	32.82	20.15	<u>48.94</u>	14.55	17.43	14.39	77.34	48.26	False
NEK, Id: 1	88.42	93.78	<u>66.13</u>	92.04	<u>96.01</u>	97.55	70.12	6.32	False
NEK, Id: 2	89.11	34.11	31.82	27.03	6.73	22.99	32.69	<u>38.31</u>	True
NEK, Id: 3	99.26	86.19	64.54	29.60	96.42	34.13	<u>98.73</u>	90.44	True
NEK, Id: 5	99.56	91.16	70.27	54.63	64.30	41.77	<u>62.23</u>	<u>98.17</u>	True
NEK, Id: 6	57.77	46.52	42.18	16.13	9.38	16.50	44.07	<u>50.94</u>	True
NEK, Id: 7	97.52	78.00	<u>62.29</u>	61.72	47.72	31.07	<u>94.97</u>	90.38	True
NEK, Id: 8	<u>96.9</u>	74.38	71.07	66.65	36.53	32.34	91.88	97.72	True
NEK, Id: 9	95.56	83.48	66.06	47.29	47.86	23.04	<u>94.62</u>	87.58	True
TODS, Id: 1	87.26	<u>89.49</u>	96.67	82.35	87.57	82.54	88.15	88.09	True
TODS, Id: 2	67.51	78.47	68.49	61.80	60.51	60.74	<u>71.35</u>	27.28	True
TODS, Id: 3	59.33	60.45	60.56	66.97	67.04	66.17	94.43	<u>85.01</u>	True
TODS, Id: 4	46.80	53.40	53.50	72.66	68.55	55.56	<u>69.22</u>	36.46	True
TODS, Id: 6	83.83	83.82	90.59	80.36	83.81	82.23	<u>89.01</u>	86.91	True
TODS, Id: 7	52.44	32.89	17.88	30.74	58.24	39.60	84.51	<u>75.74</u>	True
TODS, Id: 8	49.97	26.39	20.17	37.09	59.66	36.91	<u>59.08</u>	50.10	True
TODS, Id: 9	15.87	17.12	15.04	26.64	60.27	21.88	29.06	<u>41.48</u>	True
TODS, Id: 10	75.82	83.43	<u>81.95</u>	72.85	70.64	76.84	27.34	13.99	True
TODS, Id: 11	27.71	42.84	<u>26.33</u>	35.94	47.24	65.87	67.18	47.15	True
TODS, Id: 12	55.80	52.24	57.70	54.78	<u>67.23</u>	67.94	43.93	19.81	False
TODS, Id: 13	65.30	68.21	<u>70.95</u>	65.95	64.75	72.67	30.95	19.67	False
TODS, Id: 15	13.69	16.57	13.75	67.65	<u>52.13</u>	32.98	29.22	38.97	True

Table 7: Aggregated results on non-parametric metrics over the chosen univariate sequences with the proposed CNF & LG-LDM method.

Set	FIT	AUC-PR		AUC-ROC		VUS-PR		VUS-ROC	
		NLL	KS	NLL	KS	NLL	KS	NLL	KS
IOPS	13%	36 ± 22	19 ± 21	81 ± 12	74 ± 16	34 ± 24	15 ± 12	92 ± 8	77 ± 11
MITDB	0%	19 ± 14	15 ± 8	69 ± 7	71 ± 7	19 ± 13	16 ± 9	73 ± 7	73 ± 7
NEK	88%	61 ± 29	63 ± 36	89 ± 12	84 ± 17	74 ± 25	74 ± 29	96 ± 5	91 ± 10
Stock	100%	83 ± 14	8 ± 5	98 ± 1	51 ± 1	94 ± 9	81 ± 17	99 ± 1	92 ± 7
TODS	85%	39 ± 22	17 ± 15	77 ± 12	64 ± 11	60 ± 25	48 ± 27	89 ± 9	75 ± 16

Table 8: Aggregated results on parametric metrics over the chosen univariate sequences, except for the CV, where the critical value is used as the threshold with the proposed CNF & LG-LDM method.

Set	Standard F1		Point-adjusted F1		Event-based F1		Range-based F1		Affiliation F1		
	NLL	KS	NLL	KS	NLL	KS	NLL	KS	NLL	KS	CV
IOPS	42 ± 20	25 ± 25	80 ± 22	46 ± 39	72 ± 23	19 ± 21	38 ± 13	14 ± 9	84 ± 12	75 ± 9	69 ± 2
MITDB	25 ± 13	23 ± 10	88 ± 14	80 ± 15	56 ± 32	45 ± 20	23 ± 8	23 ± 7	86 ± 10	84 ± 6	71 ± 2
NEK	65 ± 24	67 ± 30	92 ± 12	80 ± 26	86 ± 19	71 ± 35	45 ± 16	68 ± 20	95 ± 9	90 ± 12	79 ± 10
Stock	75 ± 15	15 ± 8	76 ± 15	15 ± 8	75 ± 15	15 ± 8	77 ± 12	38 ± 18	89 ± 6	68 ± 1	66 ± 1
TODS	44 ± 19	26 ± 18	64 ± 20	39 ± 28	50 ± 22	20 ± 10	56 ± 21	34 ± 18	77 ± 7	69 ± 3	63 ± 8

B.2 Additional Multivariate Sequences Results

Table 9: Per-sequence multivariate sequence results for the VUS-PR metric. It also includes in the FIT column whether the selected model meets the trustworthiness criteria.

Sequence	PCA	CNN	FITS	TimesNet	OmniAnomaly	CNF & LG-LDM		
						NLL	KS	FIT
MITDB, Id: 1	17.62	27.78	19.17	20.00	21.97	<u>25.66</u>	20.47	False
MITDB, Id: 2	0.41	<u>1.32</u>	0.25	0.50	1.7	1.12	0.90	False
MITDB, Id: 3	2.04	<u>6.66</u>	2.55	1.58	1.41	32.49	<u>21.28</u>	False
MITDB, Id: 4	4.12	8.35	4.55	5.48	4.75	<u>7.08</u>	6.89	False
MITDB, Id: 6	1.20	<u>3.05</u>	0.99	1.57	<u>10.63</u>	3.85	19.66	False
MITDB, Id: 7	13.90	55.78	9.83	20.92	32.50	<u>48.64</u>	26.29	False
MITDB, Id: 8	10.15	<u>23.3</u>	8.95	7.50	24.24	18.62	17.93	False
MITDB, Id: 9	1.08	<u>2.15</u>	0.98	1.44	1.26	7.14	<u>5.99</u>	True
MITDB, Id: 11	11.87	<u>14.68</u>	2.26	5.24	18.73	13.40	3.69	False
MITDB, Id: 12	6.60	<u>8.2</u>	6.43	7.46	6.10	7.04	9.04	True
MITDB, Id: 13	2.80	3.27	2.80	3.00	2.79	2.59	<u>3.16</u>	False
LTDB, Id: 1	31.84	<u>60.82</u>	33.76	40.35	84.75	58.98	54.64	False
LTDB, Id: 2	19.63	<u>18.97</u>	16.68	16.39	17.11	<u>33.53</u>	36.34	False
LTDB, Id: 3	44.80	46.49	40.24	<u>51.46</u>	68.05	37.39	39.53	True
LTDB, Id: 5	1.39	4.99	0.66	0.68	<u>7.61</u>	10.04	5.10	False

Table 10: Aggregated results on non-parametric metrics over the chosen multivariate sequences with the proposed CNF & LG-LDM method.

Set	FIT	AUC-PR		AUC-ROC		VUS-PR		VUS-ROC	
		NLL	KS	NLL	KS	NLL	KS	NLL	KS
LTDB	25%	25 ± 14	21 ± 13	62 ± 16	62 ± 15	35 ± 20	32 ± 19	76 ± 14	74 ± 14
MITDB	18%	19 ± 15	12 ± 9	69 ± 11	72 ± 12	15 ± 15	12 ± 8	72 ± 11	74 ± 12

Table 11: Aggregated results on parametric metrics over the chosen multivariate sequences, except for the CV, where the critical value is used as the threshold with the proposed CNF & LG-LDM method.

Set	Standard F1		Point-adjusted F1		Event-based F1		Range-based F1		Affiliation F1		
	NLL	KS	NLL	KS	NLL	KS	NLL	KS	NLL	KS	CV
LTDB	34 ± 12	34 ± 15	77 ± 32	76 ± 11	57 ± 27	48 ± 16	22 ± 11	42 ± 24	79 ± 8	77 ± 7	73 ± 4
MITDB	26 ± 16	21 ± 11	87 ± 26	71 ± 28	77 ± 32	38 ± 33	28 ± 12	23 ± 15	91 ± 11	86 ± 9	73 ± 6

B.3 Extended framework capacity issue visualization

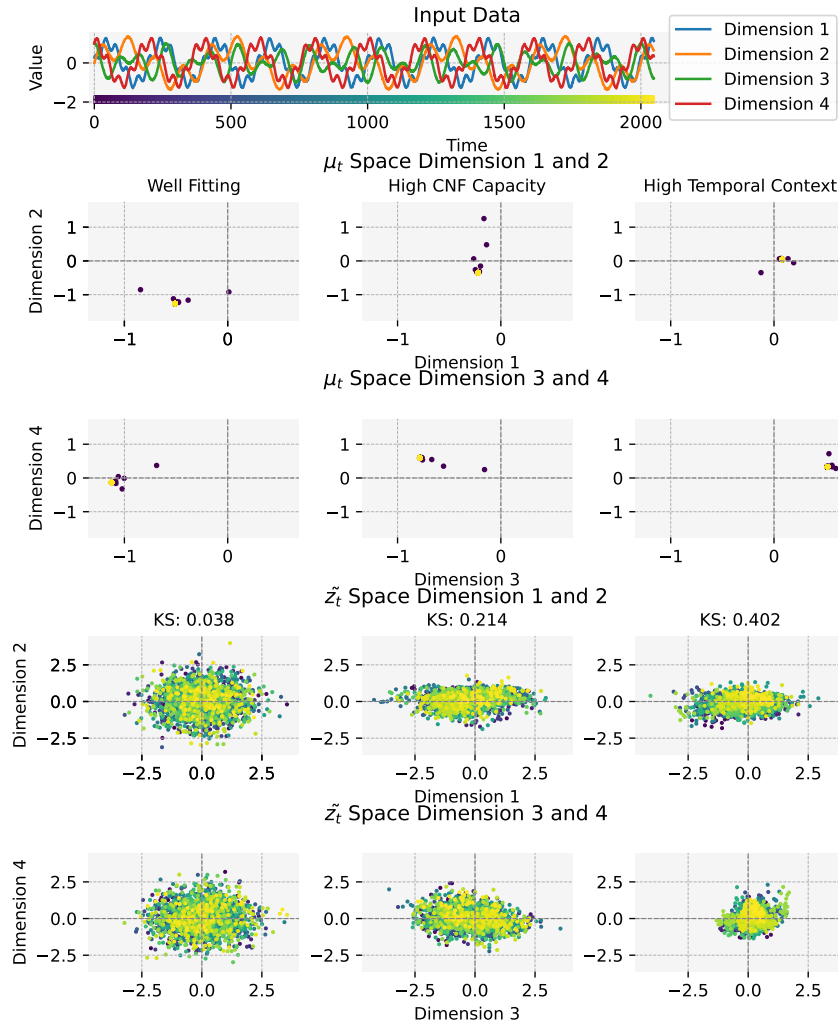


Figure 4: Example of 3 different CNF configurations and their impact on the \tilde{z}_t latent space. Row one contains the training sequence. Rows 2 and 3 contain the LG-LDM across all 4 dimensions. Rows 4 and 5 contain the \tilde{z}_t space for all 4 dimensions. The first column shows an expected fit of a Gaussian behavior. The other two columns contain CNF results with too many layers or too much temporal context. Row 4 includes in the title each model's MVN-KS value.